2023-01-1655

Ammonia Emissions from Combustion in Gasoline Engines

Abdullah U. Bajwa, Varun Shankar, Felix C. P. Leach
Department of Engineering Science, University of Oxford, UK

Abstract

Forthcoming worldwide emissions regulations will start regulating ammonia emissions from light duty vehicles. At present, most light duty vehicles are powered by gasoline spark ignition engines. Sources of ammonia emission from such engines can be in-cylinder reactions (i.e. combustion) or downstream reactions across aftertreatment devices, particularly three-way catalysts. The latter has been known to be a major source of ammonia emissions from gasoline vehicles and has been extensively investigated. The former (combustion), less so, and thus is the subject of this work. A two-zone thermodynamic spark ignition engine model with a comprehensive chemical kinetics framework (C3MechV3.3 mechanism), after being validated against experimental ammonia emissions data, is used to study ammonia formation during combustion. Reaction pathways responsible for its generation are analysed and the effects of changing the following engine operational and combustion parameters are explored: engine load, start of combustion, combustion duration, fuel-air equivalence ratio, and exhaust gas recirculation fraction.

Ammonia production was found to be slower than that of other major pollutant species - starting late during the heat release stage, peaking around the time when the cylinder pressures and temperatures were at their highest, and having a late, prolonged production stage after the end of heat release. Ammonia concentrations did not 'freeze' until late into the expansion process. Initial ammonia production was driven by three body elementary reactions involving hydrogen radicals produced from the fuel oxidation/reduction, and the late-stage production was dominated by H_2O reactions with amino radicals. The net effect of these production pathways on ammonia emissions in response to changes in engine operation was non-monotonic and depended on the dominant pathway at the particular thermal conditions. However, overall trends suggested that emissions increased when engine load increased, combustion duration shortened, combustion timing advanced, fuel-air mixture became richer and exhaust gas recirculation fraction decreased.

Introduction

Ammonia (NH_3), which exists as a gas under atmospheric conditions, is a highly toxic substance. In the UK, it has an allowable short-term (15 min) exposure limit of 35 ppm and a long-term (8 hrs) limit of 25 ppm [1]. Its adverse health effects, which include respiratory challenges, and skin, eye, and throat irritation, are well documented [2–4]. NH_3 is also a precursor to ammonium nitrate and ammonium sulphate based atmospheric aerosols, which contribute to air quality degradation. Thus, it is increasingly being regulated by automotive emissions regulations, including for sectors like light-duty vehicles where it was hitherto not regulated because of the relatively low quantities produced. Previously, it was only regulated for heavy-duty vehicles, primarily to curtail 'ammonia slip' from selective catalytic converters, which are used in lean burn (predominantly diesel) engines to manage oxides of nitrogen (NO_x) emissions. Ammonia slip occurs when excessive urea is dosed or when the catalyst temperature is low or if the catalyst has degraded over time. Ammonia slip catalysts have proven to be effective at managing these emissions.

In the recently announced Euro 7 regulations, based on a technology/fuel-agnostic approach, a 20 mg/km limit on NH_3 emissions has been proposed for all light-duty vehicles [5]. For heavy-duty vehicles, which already had NH_3 limits in the Euro 6 framework, allowable limits have been changed from 10 ppm to 65 mg/kWh. There are also expectations that upcoming regulations in China will limit NH_3 emissions to 10 mg/km [6].

The majority (around 80%) of the global light-duty vehicle fleet is currently powered by gasoline, spark-ignition (SI) engines and they are projected to be the predominant powertrain in the upcoming decade [7, 8]. Therefore, in the evolving regulatory landscape, the production mechanisms of NH_3 from such engines merit investigation. Previous SI engine studies [2, 3, 6, 9, 10] have demonstrated that three-way catalysts (TWC) play a major role in NH_3 formation by providing conditions suitable for NO_x reduction to NH_3 in a hydrogen (H_2) and carbon monoxide (CO) rich environment. Liu *et al.* [10] showed that post-TWC NH_3 concentrations were 45-72 times higher than pre-TWC levels. They attributed this to the TWC-catalysed production of H_2 from CO and H_2O in the exhaust, which reacted with NO to produce NH_3. The following reactions are considered to be the major NH_3 production pathways across TWCs [3, 9]:

$$2\,NO + 4\,CO + 2\,H_2O + H_2 \longrightarrow 2\,NH_3 + 4\,CO_2 \qquad \text{(R1)}$$

$$2\,NO + 5\,H_2 \longrightarrow 2\,NH_3 + 2\,H_2O \qquad \text{(R2)}$$

Gasoline post-TWC NH_3 emissions have been found to be higher under fuel-rich conditions than at stoichiometric conditions because under these conditions, there are greater quantities of partial products of combustion (CO and H_2) in the exhaust [2, 9]. Hence, in drive-cycle based studies sharp increases in NH_3 emissions were registered during after-treatment system (TWC, lean NO_x trap) regeneration events when combustion was momentarily richened [3]. Suarez-Bertoa *et al.* [3] found that cars compliant with more stringent emissions regulations (Euro 6) emitted more NH_3 than older ones under similar testing conditions because of NO_x storage catalyst's

regeneration events. Similarly, fuel enrichment during cold starts can also cause an increase in post-TWC NH_3 emissions [10, 11]. Emissions also increased at higher engine load levels where exhaust temperatures were high ($> 500^oC$), e.g. during rural or high speed driving, or acceleration events [3, 9, 10]. At these conditions, steam hydrocarbon reforming reactions increase CO concentration in the exhaust and through Reaction-R1, promote NH_3 formation.

Emissions of regulated pollutant species (e.g. NO_x, unburned hydrocarbons, CO) are typically managed either by treating them in the exhaust (i.e. 'after-treatment'), limiting their production (during combustion or exhaust system reactions), or a combination of the two. The primary focus of SI engine NH_3 emissions management investigations has been on the after-treatment system. This includes both its production in TWCs [3, 9, 10, 12], as well as its mitigation via post-TWC after-treatment devices like 'urea-less' (passive) selective catalytic reduction (SCR) systems [12, 13] and 'gasoline ammonia slip catalysts' [6, 14]. Passive SCR systems use NH_3 generated in TWCs to reduce NO_x and can be useful for lean-burn SI engines.

Theoretical and experimental research on ammonia oxidation has been widely studied with an increasing focus on the combustion of NH_3 as it is recognised to be a promising carbon-free fuel. Therefore, as Xu *et al.* [15] have identified, there are numerous recently published mechanisms for ammonia-relevant combustion with appropriate experimental validation. However, gasoline surrogate mechanisms with NH_3 sub-mechanisms are less common. Two mechanisms identified in the authors' literature survey were the Polimi mechanism from the Creck Modelling Group [16] and the C3MechV3.3 mechanism by the Computational Chemistry Consortium [17].

Given the low levels of NH_3 emissions that will shortly be regulated from vehicles it is important to understand both engine-out and post-TWC sources of NH_3 from gasoline vehicles. The motivation for the present work, then, is to investigate the pre-TWC, i.e. combustion, contributions to exhaust NH_3 emissions and understand the chemical pathways responsible for its production. A zero-dimensional (0D) thermodynamic model of an SI engine with detailed chemical kinetics is used to study NH_3 formation within the cylinder. The thermodynamic model permits isolated investigations of different thermodynamic and operational engine parameters on out-of-cylinder NH_3 emissions. Such investigations would not be possible in more sophisticated, spatially resolved, close-coupled, multi-physics models that simulate interactions between different thermo-chemical phenomena, e.g. changing inlet pressure (engine load) would change the turbulence characteristics of the compressed mixture and thus affect combustion phasing and/or trigger abnormal (knocking) combustion. For the same reasons, such studies would also not be feasible via engine testing. Findings from the work identify and discuss combustion based origins of NH_3 emissions. By comparing them to what is already known about NH_3 emissions originating from the exhaust system, suitable combustion and after-treatment strategies can be developed for vehicle NH_3 emissions management.

Methodology

Experimental Setup

An optically accessible single-cylinder gasoline direct injection SI engine was used to obtain the experimental data used for model validation. Whilst this setup allows for combustion and fuel spray imaging, these features were not utilized for the experiments. The engine has a crank angle marked flywheel mounted on a Control Techniques dynamometer for speed and torque control. The Taylor $DynPro_2$ system was used to remotely control the engine test cell. A crankshaft encoder with a resolution of 0.1°CA was used to trigger high-speed data acquisition with the AVL X-ion system. The spark plug and fuel injector were centrally mounted, and fuel was injected at 150 bar provided by a Heypac air-driven pump. The injection and ignition timings and duration were controlled by the Berkeley Nucleonics Corporation's (BNC) model 725 multi-trigger digital delay generator using signals from the crankshaft encoder. The cylinder pressure was measured using a Kistler Type 6041A high-speed pressure transducer. The fuel-air equivalence ratio (ϕ) was measured using a lambda sensor in the exhaust of the engine. The engine specifications and settings are presented in Table 1 and additional information can be found in previous publications [18].

Table 1: Engine specifications and settings.

Parameter	Unit	Value
Bore	mm	89.0
Stroke	mm	90.3
Displacement	cm^3	561.9
Compression ratio	-	11:1
Fuel pressure	bar	150
Valves per cylinder	-	2 intake; 2 exhaust
Injection timing	°CA aTDC	-270
Ignition timing	°CA aTDC	-46.3

The engine-out emissions were measured at a sampling rate of 5 Hz using a Fourier transform infrared spectroscopy (FTIR) gas analyser (AVL SESAM FTIR i-60). The FTIR analyser operated with a sample flow rate of 8 L/min through the 200 mL gas cell. To achieve effective gas exchange at this rate, the cell was maintained at 191°C and 800 hPa. Nitrogen gas was purged through the gas cell to normalise the background spectrum which was used to determine the absorbance. As the FTIR analyser operates at 191°C, it samples the raw exhaust without contaminating the optics with water vapour and emission constituents. The FTIR analyser sample line was also heated to 191°C, preventing losses from adsorption and condensation. A heated filter between the engine-out exhaust and the heated line removed particulate matter to prevent optical cell contamination. The measurement ranges of the components relevant to this study are summarised in Table 2.

Table 2: FTIR emissions analyser specifications for selected emissions species.

Emission component	Name	Unit	Range
Ammonia	NH_3	ppm	0-6000
Carbon monoxide	CO	ppm	0 - 100000
Carbon dioxide	CO2	ppm	0 - 200000
Nitrogen monoxide	NO	ppm	0 - 10000

The fuel used in this study was compliant with the European Standard EN228 specification for gasoline [19]. It was composed of refinery streams by Coryton with no oxygenate content. The fuel characteristics are presented in Table 3.

Table 3: Properties of the fuel used.

Property	Unit	E0
RON	-	95.5
MON	-	85.6
Density at 15°C	kg/L	0.7429
DVPE at 38°C	kPa	67.6
Net calorific value	MJ/kg	42.83
n-paraffins	% vol	9.3
iso-paraffins	% vol	43.0
olefins	% vol	10.8
naphthenes	% vol	4.1
aromatics	% vol	32.1

Experiments were carried out at ambient air intake conditions (298 ± 5 K). Fuel-air equivalence ratio (ϕ) and net indicated mean effective pressure (IMEP) were controlled by adjusting the throttle position and injection duration. Data was collected for 300 cycles once the engine had reached stable operation. The engine was operated at 1500 rpm and 2.4 to 3 bar net IMEP. Investigations were limited to such low

load cases because the optical engine cannot be safely operated at higher cylinder pressures. The equivalence ratio was varied from stoichiometric ($\phi = 1$) to rich ($\phi = 1.25$) conditions. The highest ammonia emissions ($\approx$ 8.5 ppm) were observed for the richest and highest load case ($\phi = 1.25$, 3 bar net IMEP), which is thus used for thermodynamic model validation below.

Engine Model

A model of the single-cylinder gasoline engine was developed on the commercial thermo-chemical simulator *ANSYS Chemkin* using its 'SI Engine Zonal Simulator' module. The model has a zero-dimensional and two-zone architecture, whereby it has no spatial resolution and divides cylinder content into two homogeneous zones. The cylinder mixture's thermodynamic state and composition are calculated using conservation of mass and energy equations, and a prescribed chemical kinetics mechanism [20]. The model only looks at the closed portion of the engine cycle, i.e. the period between intake valve closing (IVC) and exhaust valve opening (EVO), and splits it into three segments, namely pre-combustion compression, combustion, and post-combustion expansion. Initial temperature and pressure conditions are prescribed at IVC. A Wiebe function determines the mass flux from the unburned to the burned zone during combustion and thus the rate of combustion. Various Wiebe model arguments determine combustion parameters, including the start of combustion (SoC), combustion duration, combustion efficiency, and combustion progression rate. Wall heat transfer is simulated using the Woschni correlation [21]. Iso-octane was used as a gasoline surrogate fuel. Multi-component fuels that matched the overarching fuel composition of the gasoline fuel used were tested in the simulation and the engine performance and emissions were found to be nearly identical to those with iso-octane. Therefore, iso-octane, which is a well-established surrogate gasoline fuel, was used in the simulations to reduce computational time and avoid complications that arise from using multi-component fuels in reaction path tracking.

The surrogate fuel mechanism *C3MechV3.3*, developed by the Computational Chemistry Consortium [17], was used in the study. It is a very comprehensive mechanism with 3,761 species and 16,522 reactions. In comparison to the multitude of surrogate fuel mechanisms available in the literature, the exhaustive species and reactions of this mechanism contain the chemistry of gasoline surrogates and ammonia formation and consumption as identified by Wijeyakulasuriya *et al.* [22]. The mechanism has been validated against a wide array of binary and ternary gasoline surrogate fuels composed of n-heptane, iso-octane, and toluene to simulate fundamental combustion properties including ignition delay time and laminar burning velocity. Furthermore, the mechanism was able to predict the laminar burning velocity of a gasoline surrogate that matched the properties of a commercial gasoline, TAE7000, from TOTAL without ethanol as formulated by Dirrenberger *et al* [23]. The NH_3 sub-mechanism was taken from NUIGMech1.1. and was updated with the interaction reactions between NH_3 and C1 – C7 n-alkanes and validated against the experimental data from the literature [17, 24]. These extensive validations support the use of the *C3MechV3.3* for the purpose of this work. Additionally, as a zero-dimensional model was used, the model was able to run the full mechanism with reasonable run-times.

Model Validation

The engine model was validated at the highest load and richest fueling condition studied (3 bar net IMEP and $\phi = 1.25$) using the following validation parameters:

i Cylinder pressure and IMEP for the closed portion of cycle ($IMEP_{(IVC-EVO)}$)

ii Apparent rate of heat release (AHRR)

iii Exhaust CO emissions

iv Exhaust CO_2 emissions

v Exhaust NO emissions

Validation results are shown in Figure 1 and summarised in Table 4. NO emissions had the highest error of 12.7% followed by that for CO (11%). This could be attributed to the 0D nature of the model whereby spatial heterogeneities that exist in real engines were not simulated. Thus, ignoring combustion contributions from fuel-rich strata. Other likely sources of errors include the wall heat transfer sub-model and the chemical kinetics mechanism.

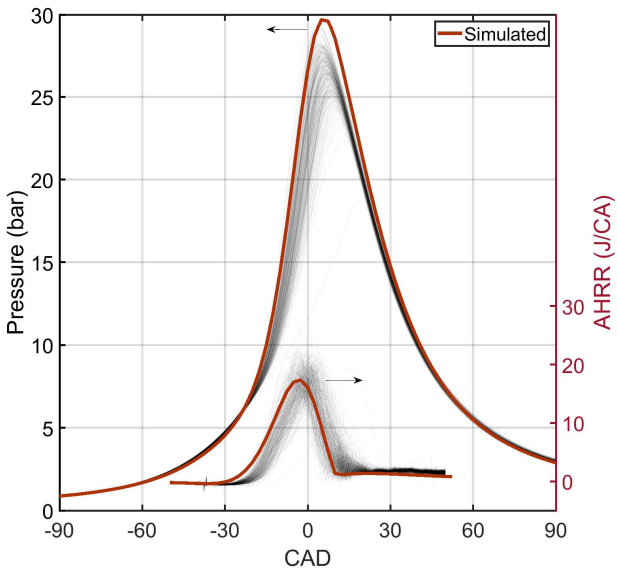

Figure 1: Simulated and experimental cylinder pressure and apparent heat release rate at 3 bar net IMEP and 1500 rpm.

NH_3 emissions prediction is also listed in Table 4. The high %-error is attributed to limitations of the 0D model and the low levels of NH_3 emissions from the engine studied. Therefore, NH_3 predictions were not used for model validation but served only as binary tests of whether NH_3 was being produced or not. Overall, the engine model was considered acceptable for the current work which focuses more on the relative trends in NH_3 emissions and less on the actual quantities.

Table 4: Comparison of simulated and measured (mean ± 1 standard deviation) values of validation parameters and exhaust NH_3. Reported error is the mean absolute percentage error.

Parameters	Experimental	Simulated	Error (%)
$IMEP_{(IVC-EVO)}$ [bar]	4.06 ± 0.25	3.83	5.7
NO [ppm]	486.3 ± 52.8	427.8	12.7
CO [ppm]	63937 ± 2481	56897	11
CO2 [ppm]	89660 ± 1742	82715	7.8
NH_3 [ppm]	8.48 ± 0.33	2.5	70.3

Modelling Study

The validated model was used to study the production of NH_3 during an engine cycle and assess the effects of various combustion timing, mixture composition, and operating point changes. Model settings varied across the different parametric sweeps are listed in Table 5. All results presented henceforth are from the engine simulation model.

Table 5: Simulation settings for the parametric modelling study.

	P_{IVC} (bar)	SoC (^{o}CA aTDC)	$CA_{10-90\%}$ (^{o}CA)	ϕ	EGR (%)
Baseline	0.65	-43	24.1	1.24	0
Load Sweep	0.65 to 1.4	-43	24.1	1.24	0
SoC Sweep	0.65	-23 to -63	24.1	1.24	0
CD Sweep	0.65	-43	17.3 to 38	1.24	0
ϕ Sweep	0.65	-43	24.1	1.03 to 1.48	0
EGR Sweep	0.65	-43	24.1	1.24	0 to 30
Higher Load	1.4	-43	24.1	1.24 to 1.43	0

Results and Discussion

NH_3 Production

The chemical kinetics based engine model is used to track the production of NH_3 in the engine cylinder during combustion for the baseline case (Table 5). Cylinder NH_3 concentration and production rate results are shown in Figure 2. For comparison and analysis, average cylinder temperature and concentrations of NO, H_2, and CO (reactants in TWC NH_3 production, Reactions-R1, R2) are shown in Figure 3. NH_3 production is slower than that of the other species. It starts almost halfway into the combustion process and takes place in two stages, indicated by the change in its production rate. Noticeable NH_3 production starts around 0^oCA before top dead centre (bTDC) and temperatures greater than 2000 K. NH_3 production rate is the highest at the point of peak cylinder temperature (2400 K at around 10^oCA aTDC). This is followed by a prolonged, slow production stage after the end of heat release. Moreover, NH_3 production does not 'freeze' until late into the expansion process (around 60^oCA aTDC).

Chemical kinetic pathways for NH_3 production are also analysed to identify important reactions and major species responsible for the observed two-stage NH_3 production behaviour. For both stages, there are three key reaction pathways that affect the ammonia rate of production as seen in Figure 4. For the first stage, the dominant reaction is Reaction-R3. It involves three-body reactions between highly reactive hydrogen (H) and amino (NH_2) radicals to produce NH_3. According to the *C3MechV3.3* mechanism, this reaction's rate expression is dependent on the pressure as well as the temperature as it has non-zero 'Troe coefficients' [25, 26]. The first stage of ammonia production occurs as the cylinder pressure peaks, therefore, it is assumed that the reaction rate for this reaction is affected by the high-pressure limit coefficients.

$$H + NH_2 + (M) \Longleftrightarrow NH_3 + (M) \quad \text{(R3)}$$

NH_2 radicals for the first ammonia production stage reaction Reaction-R3 are formed from Reactions-R4 and R5 as shown in Figure 5.

$$OH + NNH \Longleftrightarrow NO + NH_2 \quad \text{(R4)}$$

$$N_2 + H_2O \Longleftrightarrow NO + NH_2 \quad \text{(R5)}$$

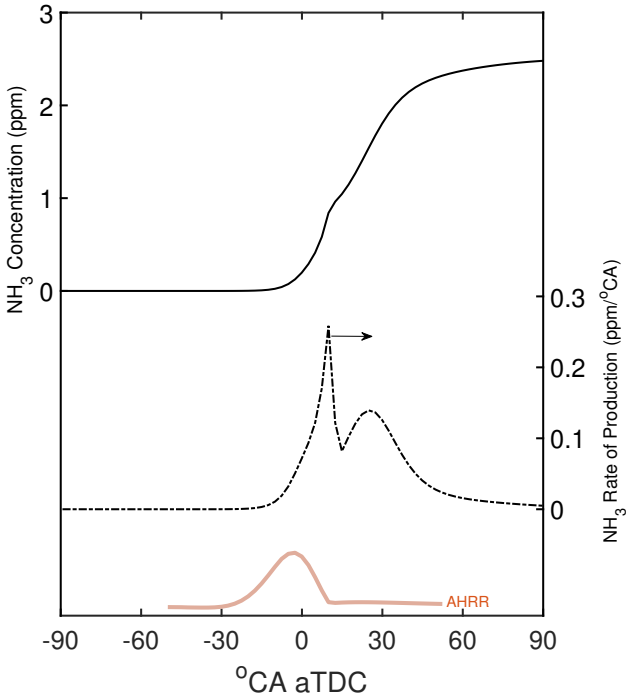

Figure 2: NH_3 production during combustion shown as average cylinder NH_3 concentration and its rate of production per ^{o}CA. AHRR curve shown at bottom to mark the combustion period.

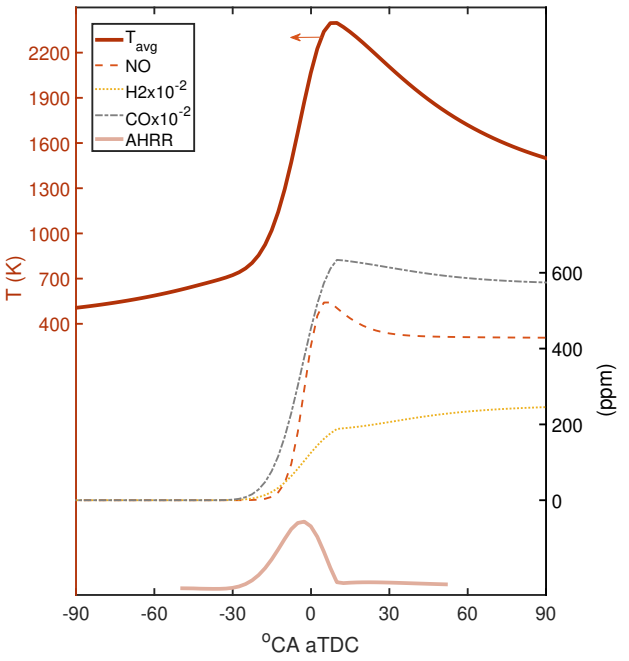

Figure 3: Simulated cylinder temperature and concentration of selected species during combustion. AHRR curve shown at bottom to mark the combustion period.

The NNH radicals are primarily formed by Reaction-R6. The hydrogen (H) radicals for both Reactions-R3 and R6 are formed from the hydrogen abstraction of the reactant species, which in this case is iso-octane (IC_8H_{18}).

$$N_2 + H \Longleftrightarrow NNH \quad \text{(R6)}$$

The second key reaction for ammonia production is Reaction-R7

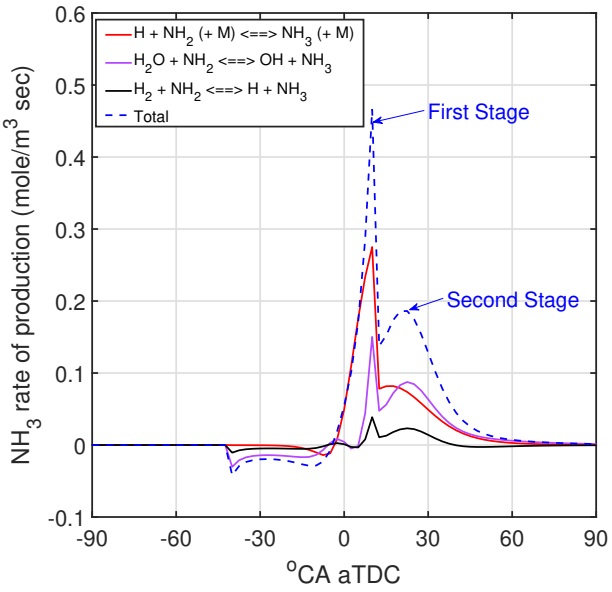

Figure 4: Top three reactions for ammonia (NH_3) production.

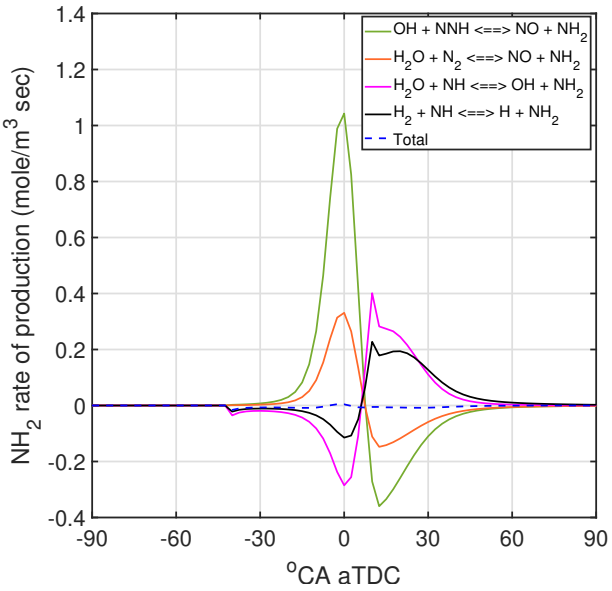

Figure 5: Top four reactions for amino radical (NH_2) production

where H_2O reacts with NH_2 radicals to form OH radicals and NH_3. For the second ammonia production stage, this reaction plays a more dominant role than Reaction-R3, as can be seen in Figure 4.

$$H_2O + NH_2 \iff OH + NH_3 \qquad (R7)$$

The hydrogen abstraction Reaction-R8 also contributes to the production of ammonia for both stages, although at a lower rate than both Reactions-R3 and R7. The production of a reactive hydrogen radical from Reaction-R8 also further propagates NH_3 production through Reaction-R3. The forward reaction is exothermic and the calculated rate constants increase significantly with temperature [27].

$$H_2 + NH_2 \iff NH_3 + H \qquad (R8)$$

NH_2 radicals participating in the second stage reactions (R7, R8) are formed via Reactions-R9 and R10, which are different to Reactions-R4 and R5 (Figure 5).

$$H_2O + NH \iff OH + NH_2 \qquad (R9)$$

$$H_2 + NH \iff H + NH_2 \qquad (R10)$$

The relative importance of key reactions during the two NH_3 production stages is summarised in Figure 6, which shows their rates of production (RoP) at selected representative crank angle locations. It can be seen that Reaction-R3 is pivotal for the first stage and Reaction-R7 is critical for the second stage reactions. Through analysing the rates of production of key species, the important reactions that affect NH_3 production are identified at the baseline condition with the reactant fuel of iso-octane.

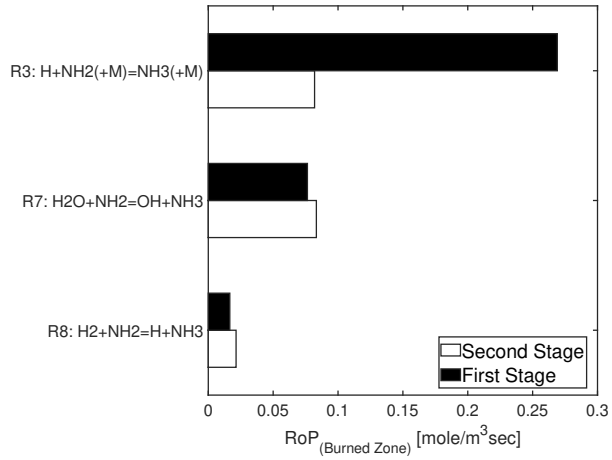

Figure 6: Rate of production of NH_3 with the baseline case comparing the first stage (CA = 10°CA aTDC) and second stage (CA = 20°CA aTDC).

Effects of Changing Engine Operating Parameters

The impact of changing engine operating and combustion parameters on NH_3 emissions is investigated next with an assessment of how the varying parameters affect important NH_3 production reactions compared to the baseline conditions.

Engine Load

To simulate the effects of increasing engine load, the start of analysis (IVC) pressure was increased from the baseline case value of 0.65 bar up to 1.4 bar. This emulates the opening of the throttle and supercharging in an SI engine. Since the fuel-air equivalence ratio was kept constant, the increased air flow caused a proportional increase in fuel supply. Hence, IMEP increased from 3.8 to 9.5 bar (Figure 7), accompanied by a rise in mixture temperature and NH_3 production (Figure 8).

Increasing load monotonically increased NH_3 emissions, taken to be cylinder NH_3 concentrations at EVO. Both the NH_3 production stages contributed almost equally to the rise in NH_3 emissions. The phasing of NH_3 production stayed unchanged as there were no significant changes in combustion phasing (AHRR in Figure 7). The primary reason for increased NH_3 emissions at higher loads was the consistently higher combustion and expansion pressure, which supported the three-body NH_3-forming reaction, Reaction-R3. At higher loads, lower amounts of OH were produced during combustion. This could have an NH_3-decreasing influence by reducing the production of NH_2 via Reactions-R4, and thus limiting feedstock for Reaction-R3. The absolute rate of production of NH_3

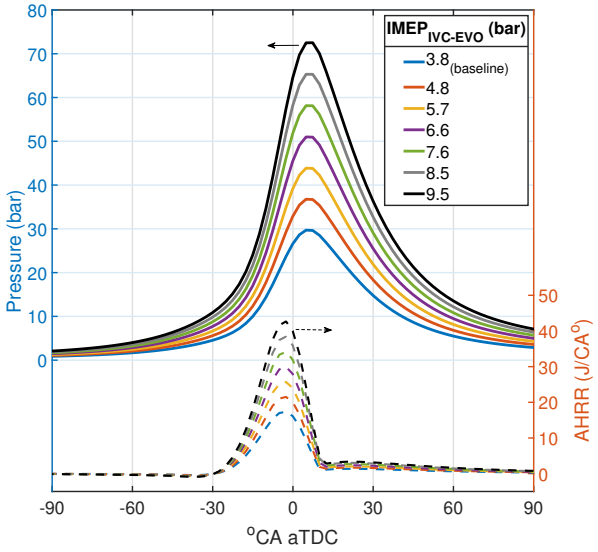

Figure 7: Simulated cylinder pressure and apparent heat release rate at different engine loads.

from the three-body reaction Reaction-R3 increased more than eleven-fold at the peak temperature point (≈10^{o}CA aTDC) when IMEP increased from the baseline case to 9.5 bar. The corresponding production from the second stage reaction, Reaction-R7, increased around five-fold, likely because of an increase in forward reaction rates at higher temperatures.

As mentioned in the introduction, incidentally, NH_3 production from TWC reactions also increases at higher loads. The underlying mechanisms are, however, different.

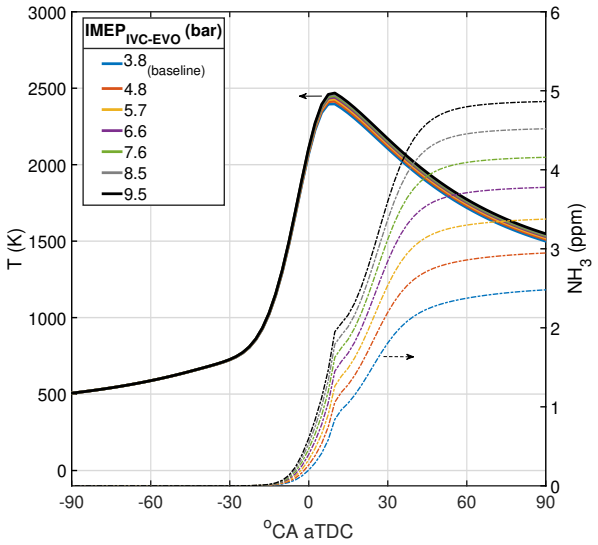

Figure 8: Simulated cylinder temperature and NH_3 concentration at different engine loads.

Combustion Phasing

Effects of combustion phasing were investigated by changing the combustion duration, defined as 10 to 90% mass faction burn period ($CA_{10-90\%}$), and the location of the start of combustion (SoC).

User-prescribed SoC in the thermodynamic model can be considered a proxy for spark timing in SI engines. SoC was swept from 23 to 63^{o}CA bTDC as shown in Figure 9. Advancing combustion increased cylinder pressure (Figure 9) and temperature (Figure 10). NH_3 emissions increased up to SoC of 43^{o}CA bTDC, but further advancement resulted in a reduction in NH_3 emissions (Figure 10). The decrease was characterised by an earlier cessation of the first stage NH_3 formation reactions, coupled with a delayed start of the second stage reactions.

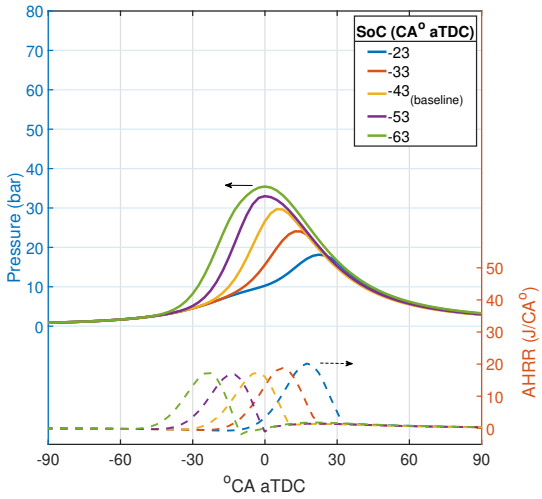

Figure 9: Simulated cylinder pressure and apparent heat release rate at different SoC timings.

The observed trends can be attributed to the interplay between the following NH_3 production supporting and discouraging influences: higher pressures increased NH_3 production from three-body reactions (Reaction-R3) and increased OH production at higher temperatures (Figure 11), which increased the production of NH_2 via Reaction-R4 and thus further increased NH_3 production from Reaction-R3. Simultaneously, the rapid increase in temperature increased the backward reaction rate for the three-body reaction Reaction-R3 as well as that of stage two NH_3 production reaction Reaction-R7. The most delayed combustion cases (SoC 23^{o}CA bTDC) did not exhibit first stage NH_3 production, likely because of very low combustion pressures.

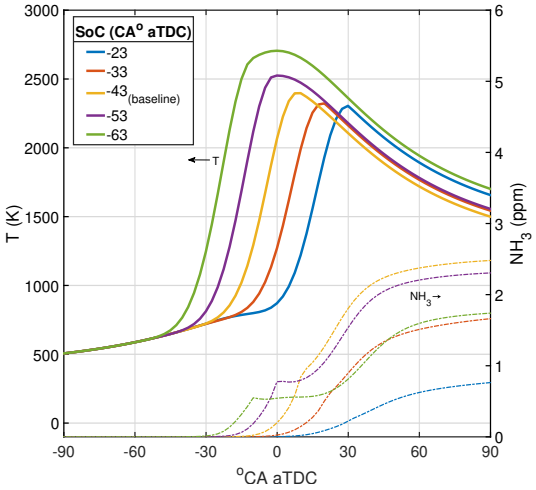

Figure 10: Simulated cylinder temperature and NH_3 concentration at different SoC timings.

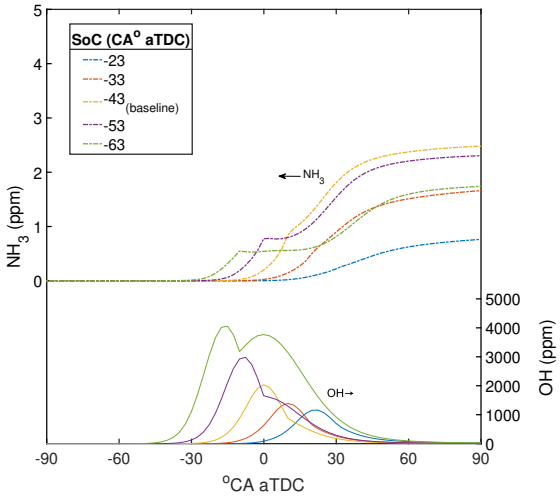

Figure 11: Simulated NH_3 and OH concentration at different SoC timings.

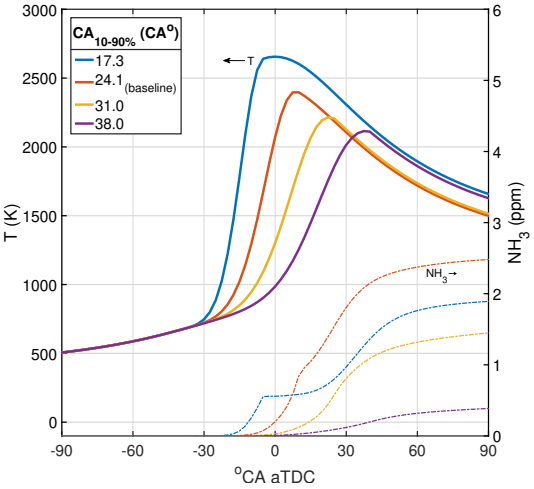

Figure 13: Simulated cylinder temperature and NH_3 concentration for different combustion duration cases.

Overall, advancing SoC from 23 to 63^{o}CA bTDC led to a more significant increase in second stage NH_3 production than from the first stage. NH_3 production from Reaction-R7 increased more than five-fold, whilst that from Reaction-R3 increased 1.4 times. This is opposite to what was observed for the load sweep, likely because of milder pressure and more extreme temperature rise.

Combustion duration ($CA_{10-90\%}$), which indexes the speed of combustion (specifically, flame propagation for SI engines), was swept from 17.3 to 38^{o}CA as shown in Figure 12. Elongating combustion duration (with SoC held constant) lowered combustion pressures and temperatures (Figures 12, 13). Similar to the SoC sweep, the observed NH_3 production changes can be explained by variations in NH_3 formation mechanisms resulting from changes in cylinder pressure and temperature, and their effects on reaction rates of important reactions (Reaction-R3, R7) and the production of OH radicals (Figure 14).

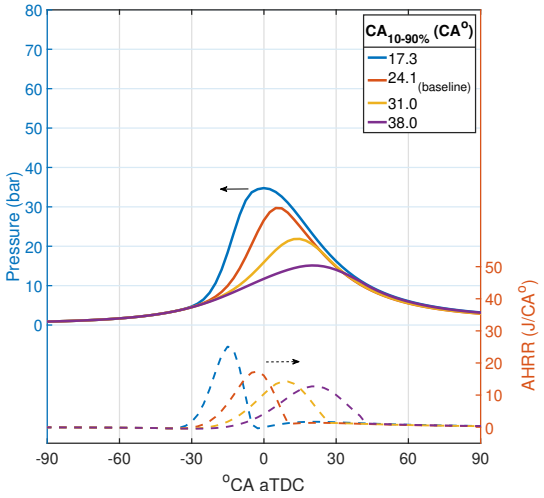

Figure 12: Simulated cylinder pressure and apparent heat release rate for different combustion duration cases.

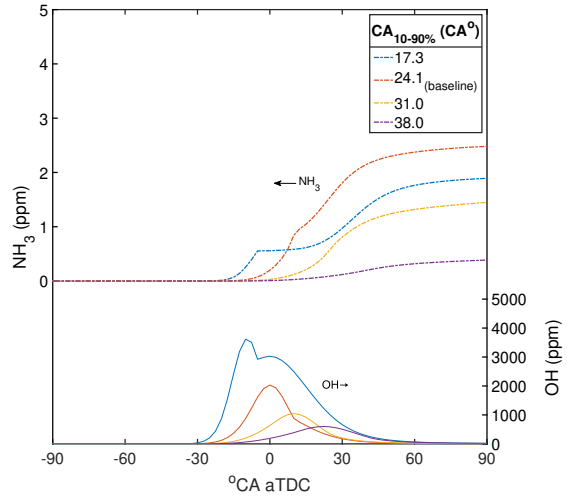

Figure 14: Simulated NH_3 and OH concentration for different combustion durations.

Mixture Composition Effects

Fuel air equivalence ratio (ϕ) was swept from 1.03 to 1.48. At conditions leaner than $\phi = 1.03$, no NH_3 was produced and they are therefore not shown. Fuel enrichment up to $\phi = 1.38$ led to a significant increase in NH_3 emissions of around 4.5 ppm, which was followed by a drop in emissions for the very rich cases ($\phi > 1.4$). This is shown in the NH_3 production and emissions results in Figures 15 and 16, respectively. Fuel enrichment produced very small changes in cylinder pressure, while producing a more pronounced, yet still mild compared to load and combustion phasing sweeps, reduction in cylinder temperature. Correspondingly, the OH concentration decreased, while H and H_2O concentrations initially increased and then decreased for the very rich mixtures (Figure 16).

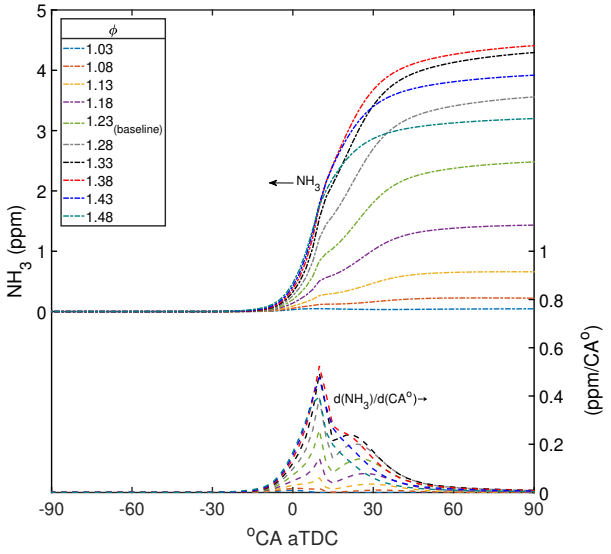

Figure 15: NH_3 production during combustion of different ϕ mixtures.

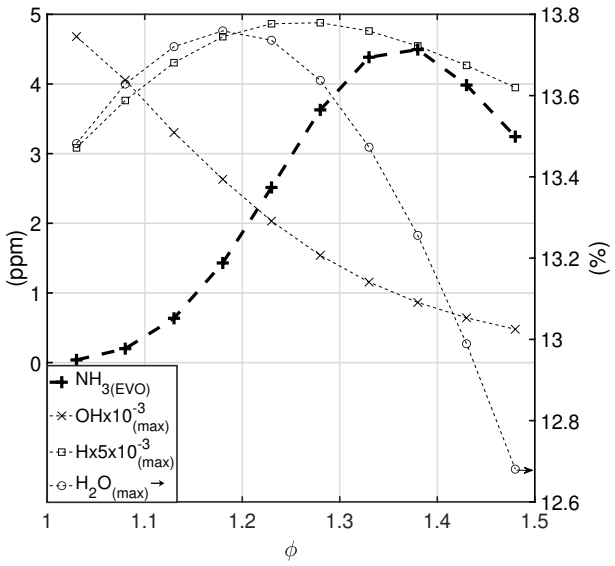

Figure 16: Change in peak cylinder OH, H, and H_2O concentrations, and NH_3 concentration at EVO for different ϕ mixtures.

The initial increase in NH_3 emissions upon enrichment can be attributed to increased production from Reaction-R3 and R7 as more H and H_2O are available, respectively. The reduction in OH along with that in H_2O at rich conditions, respectively, led to a reduction in NH_2 production from Reaction-R4 during the first stage and from Reaction-R9 during the second stage. Thus, decreasing NH_3 production for rich mixtures. At rich conditions, NH_3 production was also limited directly by reduction in H_2O and H availability.

The extremely rich conditions at which NH_3 emissions decrease are unlikely to be encountered in modern SI engines. Therefore, the combustion NH_3 emission trends are generally similar to those of post-TWC emissions, where too, rich operation increased NH_3 emissions. Thus, stoichiometric or lean operation can help reduce NH_3 emissions from both combustion and post-combustion (exhaust) reactions.

The effects of increasing exhaust gas recirculation (EGR) level were investigated by changing the composition of the trapped mixture from having no residual combustion gases to residual gases constituting 30% of the total mixture on a molar basis. The results, shown in Figure 17, reveal that increasing EGR levels lowered NH_3 emissions. The reduction was primarily caused by the weakening of three-body NH_3 forming reactions because of a reduction in cylinder pressure and availability of H radicals. There were also secondary contributions from reduced NH_3 production via Reaction-R7, likely because of a reduction in cylinder temperature with increasing EGR.

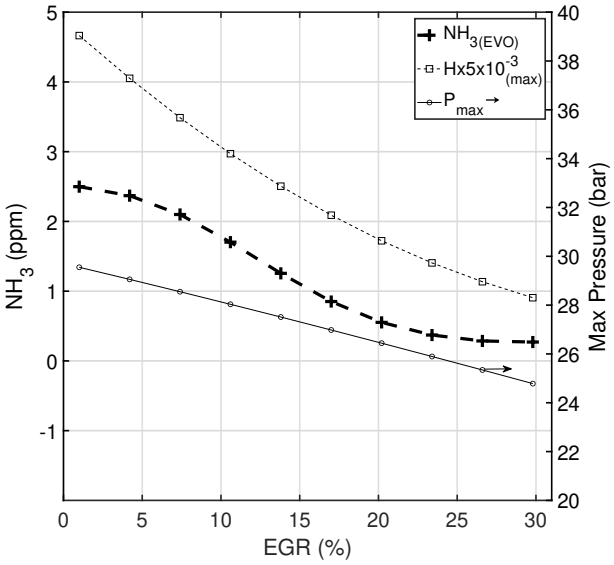

Figure 17: Change in peak cylinder pressure and H concentration, and NH_3 concentration at EVO with changing EGR levels.

Combined Effects

The most significant increase in NH_3 emissions resulted from increasing engine load (Figure 8) and ϕ (Figure 16). An extreme NH_3 emissions scenario is thus constructed with an initial pressure of 1.4 bar, which was the highest load case in the load sweep, and a ϕ of up to 1.43, which yielded the highest NH_3 emissions in the ϕ-sweep. The results, shown in Figure 18, demonstrate that at high pressure and rich conditions, NH_3 emissions rise to almost 12 ppm - a five-fold increase compared to the baseline case (ϕ = 1.24, P_{IVC} = 0.65 bar). At such conditions, the NH_3 forming three-body reactions are very active because of high pressures and concentrations of H radicals.

To assess how the simulated NH_3 emission levels compare to regulatory limits, NH_3 emissions factor in mg/km is estimated for the peak value of 11.4 ppm. An approach adapted from Leach [28] is used for a popular light-duty vehicle (Vauxhall Corsa Design, 1.2-litre) under 'typical' urban driving operation. For an assumed volumetric efficiency range of 70 - 120% (supercharged), 2 - 3.6 mg/km of NH_3 is emitted. Even though the emissions fall within the 20 mg/km Euro 7 limit, at around 20% of the limit, they cannot be considered negligible. Combustion NH_3 emissions can potentially become significant at higher engine load points (>20 bar net IMEP). Moreover, it has to be remembered that the current engine simulation model underestimated NH_3 emissions for the baseline case (Table 4). In addition, the NH_3 emissions considered in this work are engine-out only and NH_3 emissions generated over any aftertreatment devices are not considered. Therefore, actual peak NH_3 emissions could be even higher.

A summary of the overall effects of all the simulated cases is presented in Figure 19, which compares CO and NH_3 emissions. Drive-cycle based gasoline vehicle studies have reported strong,

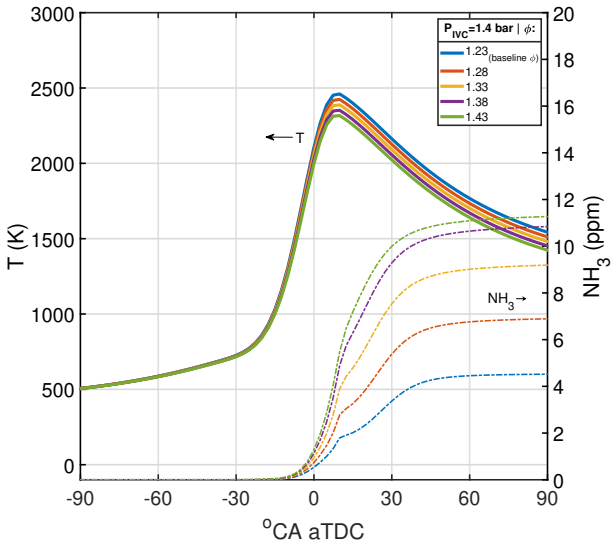

Figure 18: Simulated cylinder temperature and NH_3 concentration for different ϕ mixtures at the the higher load point.

positive correlations between post-TWC CO and NH_3 emissions, and CO has thus been regarded as an NH_3 precursor [9, 10, 29]. Figure 19 shows that for out-of-cylinder (pre-TWC) emissions, while a strong positive correlation might exist for the (baseline and increased load) ϕ sweeps, such correlations are not observed when only load, combustion phasing, combustion duration or EGR levels are changed.

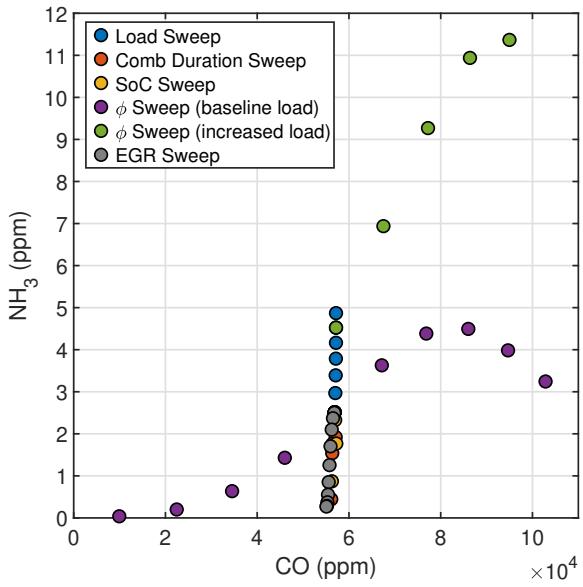

Figure 19: Changes in simulated out-of-cylinder NH_3 and CO emissions for the entire parametric study.

Summary and Conclusions

A zero-dimensional thermodynamic model of a gasoline spark ignition engine, after being validated, was used to observe the effects of thermodynamic engine performance parameters in isolation on NH_3 emissions. NH_3 production was found to take place in two stages with the following reactions controlling its production in each stage, respectively:

$$H + NH_2 + (M) \Longleftrightarrow NH_3 + (M)$$

$$H_2O + NH_2 \Longleftrightarrow OH + NH_3$$

The production of NH_3 reactions depended on the reaction rate coefficients at the particular thermal (including pressure for the first stage reaction) conditions and availability of reactants.

Parametric sweeps were carried out for the following engine operating and combustion parameters: engine load, start of combustion, combustion duration, fuel-air equivalence ratio, and exhaust gas recirculation fraction; and observed changes in NH_3 emissions were analysed using the important production pathways identified. Increasing engine load increased NH_3 emissions, primarily driven by heightened three-body reaction activity. Changes in combustion phasing affected NH_3 production through changes in three-body reaction activity and the availability of OH radicals. NH_3 emissions increased as mixtures were enriched to $\phi = 1.38$, but further enrichment led to a reduction in NH_3 emissions. Increasing EGR had the opposite effect and NH_3 emissions approached near-zero levels at EGR greater than 20%. At high load and rich conditions, a significant amount of NH_3 was produced from combustion processes (a five-fold increase compared to the baseline case). This could have implications for transient engine operation and aftertreatment system regeneration.

The study showed that potentially significant quantities of NH_3 can originate from combustion reactions in the cylinder and that the formation mechanisms of cylinder NH_3 are different from NH_3 formed in the exhaust system (TWCs). However, incidentally, both mechanisms are the strongest at high loads and rich conditions. In future work, the experimental test campaign should be extended to higher engine load points that are more representative of real driving conditions, and the performance of the thermodynamic engine model should be assessed at such conditions. Moreover, other chemical kinetics mechanisms that include NH_3 should be used to study NH_3 production mechanisms and engine-out NH_3 emissions.

Abbreviations

ϕ	Equivalence ratio
0D	Zero-dimensional
AHRR	Apparent heat release rate
aTDC	After top dead centre
bTDC	Before top dead centre
CA	Crank angle
EGR	Exhaust gas recirculation
EVO	Exhaust valve opening
FTIR	Fourier transform infrared spectroscopy
IMEP	Indicated mean effective pressure
IVC	Inlet valve closing
M	Third body in three body reactions
NH_3	Ammonia
NO_x	Oxides of nitrogen
RoP	Rate of production
rpm	Revolutions per minute
SCR	Selective catalytic reduction
SI	Spark ignition
SoC	Start of combustion
TDC	Top dead centre
TWC	Three way catalyst

Contact Information

Felix Leach
Department of Engineering Science,
University of Oxford,
Parks Rd,
Oxford,
OX1 3PJ,
UK
felix.leach@eng.ox.ac.uk

References

[1] "Eh40/2005 workplace exposure limits", Health and Safety Executive, Tech. Rep., Jan. 2020. [Online]. Available: https://www.hse.gov.uk/pubns/books/eh40.htm.

[2] Q. Zhang, M. Li, S. Shao, and G. Li, "Ammonia emissions of a natural gas engine at the stoichiometric operation with twc", *Applied Thermal Engineering*, vol. 130, pp. 1363–1372, 2018, ISSN: 1359-4311. DOI: j.applthermaleng.2017.11.098.

[3] R. Suarez-Bertoa, A. Zardini, and C. Astorga, "Ammonia exhaust emissions from spark ignition vehicles over the new european driving cycle", *Atmospheric Environment*, vol. 97, pp. 43–53, 2014, ISSN: 1352-2310. DOI: 10.1016/j.atmosenv.2014.07.050.

[4] "Ammonia incident management", Public Health England, Tech. Rep., Jan. 2019.

[5] A. Joshi, "Year in review: Progress towards decarbonizing transport and near-zero emissions", in *WCX SAE World Congress Experience*, SAE International, 2023. DOI: 10.4271/2023-01-0396.

[6] L. Xu, F. Zhao, H. Wei, P. Zhao, W. Qian, and M. Qian, "The development of a zeolite-based cold-start catalyst (csc) for a conventional china 6b vehicle in meeting the next more stringent chinese vehicle emission standards", in *WCX SAE World Congress Experience*, SAE International, 2023. DOI: 10.4271/2023-01-0233.

[7] K. Senecal and F. Leach, *Racing Toward Zero: The Untold Story of Driving Green*. SAE International, 2021. DOI: 10.4271/9781468601473.

[8] Statista. "Breakdown of global car sales in 2019 and 2030, by fuel technology". (2020).

[9] A. Żółtowski and W. Gis, "Ammonia emissions in si engines fueled with lpg", *Energies*, vol. 14, no. 3, 2021, ISSN: 1996-1073. DOI: 10.3390/en14030691.

[10] Y. Liu, Y. Ge, J. Tan, H. Wang, and Y. Ding, "Research on ammonia emissions characteristics from light-duty gasoline vehicles", *Journal of Environmental Sciences*, vol. 106, pp. 182–193, 2021, ISSN: 1001-0742. DOI: 10.1016/j.jes.2021.01.021.

[11] Z. Stepień, J. Czerwinski, P. Comte, and S. Oleksiak, "Nanoparticle and non-legislated gaseous emissions from a gasoline direct-injection car with ethanol blend fuels and detergent additives", *Energy & Fuels*, vol. 30, no. 9, pp. 7268–7276, 2016. DOI: 10.1021/acs.energyfuels.6b00583.

[12] K. Ramanathan, C. S. Sharma, and C. H. Kim, "Global kinetics for ammonia formation and oxidation reactions in a commercial three-way catalyst", *Industrial & Engineering Chemistry Research*, vol. 51, no. 3, pp. 1198–1208, 2012. DOI: 10.1021/ie2017866.

[13] Q. Lin, P. Chen, and V. Y. Prikhodko, "Experimental Study and Model Predictive Control of a Lean-Burn Gasoline Engine Coupled With a Passive Selective Catalytic Reduction System", *Journal of Dynamic Systems, Measurement, and Control*, vol. 141, no. 9, May 2019, 091008, ISSN: 0022-0434. DOI: 10.1115/1.4043269.

[14] M. Nilsson, H. Birgersson, W. Müller, P. Gabrielsson, and E Senar Serra, "Next generation global emission solution platform with dual urea dosing—meeting future emission and efficiency requirements", in *42nd International Vienna Motor Symposium*, 2021.

[15] L. Xu, Y. Chang, M. Treacy, Y. Zhou, M. Jia, and X.-S. Bai, "A skeletal chemical kinetic mechanism for ammonia/n-heptane combustion", *Fuel*, vol. 331, p. 125 830, 2023, ISSN: 0016-2361. DOI: 10.1016/j.fuel.2022.125830.

[16] E. Ranzi, A. Frassoldati, A. Stagni, M. Pelucchi, A. Cuoci, and T. Faravelli, "Reduced kinetic schemes of complex reaction systems: Fossil and biomass-derived transportation fuels", *International Journal of Chemical Kinetics*, vol. 46, pp. 512–542, 9 Sep. 2014, ISSN: 1097-4601. DOI: 10.1002/KIN.20867.

[17] S. Dong *et al.*, "A new detailed kinetic model for surrogate fuels: C3mechv3.3", *Applications in Energy and Combustion Science*, vol. 9, p. 100 043, 2022, ISSN: 2666-352X. DOI: 10.1016/j.jaecs.2021.100043.

[18] V. Shankar and F. Leach, "Effects of oxygenate and aromatic content on engine-out aldehyde emissions from pure, binary, and ternary mixtures of ethanol, toluene, and iso-octane", in *JSAE/SAE Powertrains, Energy and Lubricants International meeting*, SAE International, 2023.

[19] E. Standard, "Automotive fuels; unleaded petrol-requirements and test methods", 2008.

[20] ANSYS, "Ansys Chemkin-Pro® Theory Manual", 2022.

[21] G. Woschni, "A universally applicable equation for the instantaneous heat transfer coefficient in the internal combustion engine", in *National Fuels and Lubricants, Powerplants, Transportation Meetings*, SAE International, 1967. DOI: 10.4271/670931.

[22] S. Wijeyakulasuriya *et al.*, "Enabling powertrain technologies for euro 7/vii vehicles with computational fluid dynamics", *Transportation Engineering*, vol. 9, p. 100 127, 2022, ISSN: 2666-691X. DOI: 10.1016/j.treng.2022.100127.

[23] P. Dirrenberger *et al.*, "Laminar burning velocity of gasolines with addition of ethanol", *Fuel*, vol. 115, pp. 162–169, 2014, ISSN: 0016-2361. DOI: 10.1016/j.fuel.2013.07.015.

[24] P. Glarborg, J. A. Miller, B. Ruscic, and S. J. Klippenstein, "Modeling nitrogen chemistry in combustion", *Progress in Energy and Combustion Science*, vol. 67, pp. 31–68, 2018, ISSN: 0360-1285. DOI: 10.1016/j.pecs.2018.01.002.

[25] R. G. Gilbert, K. Luther, and J. Troe, "Theory of thermal unimolecular reactions in the fall-off range. ii. weak collision rate constants", *Berichte der Bunsengesellschaft für physikalische Chemie*, vol. 87, pp. 169–177, 2 Feb. 1983, ISSN: 0005-9021. DOI: 10.1002/BBPC.19830870218.

[26] R. Design, "Chemkin Theory Manual Chemkin ® Software", 2016.

[27] T. L. Nguyen and J. F. Stanton, "Ab initio thermal rate coefficients for H + NH 3 ¡==¿ H 2 + NH 2", *International Journal of Chemical Kinetics*, vol. 51, 5 2019, ISSN: 10974601. DOI: 10.1002/kin.21255.

[28] F. Leach, "A negative emission internal combustion engine vehicle?", *Atmospheric Environment*, vol. 294, p. 119 488, 2023, ISSN: 1352-2310. DOI: 10.1016/j.atmosenv.2022.119488.

[29] R. Suarez-Bertoa, A. Zardini, H. Keuken, and C. Astorga, "Impact of ethanol containing gasoline blends on emissions from a flex-fuel vehicle tested over the worldwide harmonized light duty test cycle (wltc)", *Fuel*, vol. 143, pp. 173–182, 2015, ISSN: 0016-2361. DOI: 10.1016/j.fuel.2014.10.076.

Acknowledgements

This research was funded in whole or in part by the Engineering and Physical Sciences Research Council Prosperity Partnership, grant number EP/T005327/1. For the purpose of Open Access, the author has applied a CC BY public copyright licence to any Author Accepted Manuscript (AAM) version arising from this submission. The Prosperity Partnership is a collaboration between Jaguar Land Rover, Siemens Digital Industries Software, the University of Bath, and the University of Oxford. The authors would also like to thank the Dept. of Engineering Science technicians and maintenance teams for facilities support.Varun Shankar acknowledges the scholarship support of The Rhodes Trust. This publication also arises from research funded by the John Fell Oxford University Press Research Fund. Due to confidentiality agreements with research collaborators, data supporting this paper can only be made available to bona fide researchers subject to a non-disclosure agreement. Details of the data and how to request access are available from the "Oxford Research Archive" repository at https://ora.ox.ac.uk/.